Quaternary sedimentation on the Makran margin: turbidity current–hemipelagic interaction in an active slope-apron system

DORRIK A. V. STOW[1], ALI R. TABREZ[2] & MARTEEN A. PRINS[3]

[1]*Southampton Oceanography Centre, University of Southampton, Southampton SO14 3ZH, UK (e-mail: davs@soc.soton.ac.uk)*

[2]*National Institute of Oceanography, Karachi, Pakistan*

[3]*Faculty of Earth Sciences, Vreije Universiteit, 1081 HV Amsterdam, Netherlands*

Abstract: The Makran slope-apron system is a stepped convergent margin across an active subduction complex. Shallow penetration piston cores have been recovered from the upper-slope region, three mid-slope basins and the abyssal plain. At most sites the upper 5–14 m of cored section is dominated by fine-grained, thin- to medium-bedded turbidites, averaging 5–10 turbidite events per metre of section. Oxygen isotope stratigraphy yields mean sedimentation rates of 50–95 cm ka^{-1} and a turbidite frequency of one event per 200–300 a. The upper-slope site has fewer turbidites and a greater proportion of hemipelagic mud. Fine-grained turbidite sequences are common, with top-cut-out and base-cut-out sequences most evident. Markov chain analysis of the transition between turbidite divisions confirms the normal T0–T8 order of sequence divisions. In some cases there is an upward gradation into a hemiturbidite facies. The range of turbidite bed thicknesses can be approximated by both power-law and log-normal distributions, typical of seismic triggering on an active margin, or of frequent river-flood sediment input. Small-scale vertical variations of turbidite bed thickness recognized by autocorrelation techniques can be interpreted as the result of bed-relief compensation effects (compensation cycles). The lateral distribution of both turbidites and hemipelagites is influenced by sediment focusing along pathways between slope basins. At a larger scale, climate, sea-level and tectonic effects have all played an important role in shaping margin sedimentation.

The continental margin off Pakistan and Iran is the offshore extension of the Makran accretionary complex, where oceanic crust of the Gulf of Oman has been subducting under the Asian continent since late Cretaceous time (Arthurton *et al.* 1982; White 1982). Progressive accretion onto the Asian plate has produced a topography of uplifted basins and intervening ridges aligned parallel to the Makran coast (White 1982, 1989). The mechanics and style of deformation has recently analysed on the basis of detailed swath-bathymetric data acquired by Kukowski *et al.* (2001). The influence of mud volcanoes throughout the accretionary complex has been well documented (e.g. Wiedicke *et al.* 2001).

Most previous studies of deep marine sedimentation in the NW Indian Ocean have concentrated on the faunal response to wind-induced upwelling, and on aeolian dust transport in relation to monsoonal climate (e.g. Prell & Streeter 1982; Prell *et al.* 1989, 1990; Clemens & Prell 1990). Recent palaeoceanographic studies in the area include those of Schulz *et al.* (1996, 1998), Reichart *et al.* (1997, 1998), 5 and Luckge *et al.* (2001). The close correspondence of climate change to style of sedimentation has been amply demonstrated by these studies. Several regional studies have also focused on clay mineral distribution in the Arabian Sea in particular (e.g. Kolla *et al.* 1976, 1981; Faugeres & Gonthier (1981); Sirocko & Lange 1991). More recently, Prins & Postma (2000) and Prins *et al.* (2000*a, b*) have attempted to distinguish between the effects of climate, sea level and tectonics on sedimentation on the Makran slope and Indus Fan.

The aim of this paper is to further document the nature of Pleistocene to Holocene sedimentation on the Makran margin, based on a series of piston five cores taken as part of the Netherlands Indian Ocean Programme (NIOP 468, 469, 470, 471 and 472) and limited 3.5 kHz data recovered from a north–south slope transect south of Gwadar. The survey area and core locations are shown in Fig. 1. Visual and X-radiograph descriptions of split cores were followed by standard textural and compositional sediment analyses, together with dating by oxygen isotope and magnetostratigraphic techniques. The full dataset has been

From: CLIFT, P.D., KROON, D., GAEDICKE, C. & CRAIG, J. (eds) 2002. *The Tectonic and Climatic Evolution of the Arabian Sea Region*. Geological Society, London, Special Publications, **195**, 219–236.
0305-8719/02/$15.00

presented by Tabrez (1995). A previous paper outlines the characteristics of hemipelagites from the Makran margin (Stow & Tabrez 1998). This paper concentrates more on details of the turbidite sedimentation. The work by Prins *et al.* (2000*b*), based on the same suite of cores (Prins 1999), focuses on the principal controls on terrigenous sediment supply.

Morphotectonic framework

The Makran continental margin forms the seaward extremity of an accretionary sediment prism that extends several hundreds of kilometres inland (White 1977; White & Louden 1982; Minshull & White 1989). This marks the zone of convergence between oceanic lithosphere of the Arabian plate and continental lithosphere of the Eurasian plate, with an estimated subduction rate of 3–5 cm a^{-1} (Quittmeyer & Kafka 1984). Because of the highly active nature of this margin, tectonic activity has undoubtedly played a key role in shaping the morphology and influencing the distribution and deposition of sediments.

Where the margin has been studied in detail by both continuous seismic reflection profiling and wide-angle seismic data, it is seen to comprise a series of ridges and intervening basins aligned parallel to the Makran coast (White & Ross 1979; Minshull & White 1989; Kopp *et al.* 2000; Kukowski *et al.* 2001). The development of this topography is exemplified in the extreme south of the margin, where gently dipping sediments beneath the abyssal plain are seen to be deformed in a frontal fold (currently at 24°10′N) to a maximum amplitude of 400 m. When crustal shortening can no longer be accommodated in this way, thrusting occurs and the frontal fold block is uplifted to over 1 km above the abyssal plain. The focus of folding moves further offshore and a proto-thrust with negligible offset marks a zone of weakness where the next thrust is likely to occur (White 1982).

A distinctive sea-floor topography is generated in this way as sediment slabs are scraped off the subducting Arabian plate. The accreted sediment is deformed into a series of imbricate thrust slices with small slope basins formed between each successive thrust slice. These basins contain an infill of post-depositional sediments derived from the nearby landmass and supplemented by slumping from the adjacent ridges, which in some cases have slopes as high as 20° (Kukowski *et al.* 2001). These basin sediments provide evidence for continued tectonic activity in that bedding plane dips increase with depth, and fault drag is shown by curvature of reflectors into the thrust planes.

Within such an active morphotectonic system, the development of a downslope drainage pattern is markedly affected by both the slope-parallel ridge–basin morphology and the constant changes to that morphology induced by tectonic activity. In some parts, including the study area, there are a series of incipient channels and channel-like pathways connecting basins and other topographic lows in a pattern analogous to a continental trellis drainage network. In other parts, for example further east from the study area (Kukowski *et al.* 2001), one or two tributary networks feed into more major canyons that have become well established (e.g. Save and Shadi Canyons). The variation in channel orientation and relief is nevertheless significantly affected by the local morphology.

Stratigraphic framework

The five piston cores recovered from the Makran margin for this study are between 5 and 14 m in length, and so penetrate only the topmost part of the stratigraphic succession. They can be correlated on the basis of distinctive lithostratigraphic characteristics, and then dated using a combination of stable oxygen isotopes and magnetostratigraphy. This latter work (by Tabrez 1995) has been more precisely calibrated by accelerating mass spectrometry (AMS) ^{14}C dates obtained by Prins (1999) and Prins & Postma (2000).

The two principal sediment facies encountered are turbidites and hemipelagites. There is a marked change in the turbidite facies, clearly recognized in four out of five cores, from a lower unit of closely spaced thin-bedded turbidites, to an upper unit of thicker-bedded but less abundant turbidites (Horizon A, Fig. 2a). This change coincides with a marked minimum in mean grain size of both the turbidite and hemipelagite facies evident in all cores (Fig. 2b). Age dating places this horizon at around 7500 a BP.

Oxygen isotope stable analyses were carried out on the planktonic foraminifer *Neogloboquadrina dutertrei*picked from some 80 closely spaced samples (every 10–20 cm in hemipelagite facies) from two long cores (469 and 472). These results are illustrated in Fig. 2b together with the standard ^{18}O isotope curve for the Arabian Sea from Sirocko *et al.* (1991). The marked decrease in ^{18}O values at about 5 m depth in core 469 represents the transition from the last glacial period to the Holocene interglacial (Marine Isotopic Stage MIS 2 to 1, Termination I). The distinctive two-step change in this core probably corresponds to Termination Ia and Ib, so that the lower ^{18}O values between Ia and Ib would represent the Younger Dryas event (Steens *et al.* 1991). The relatively

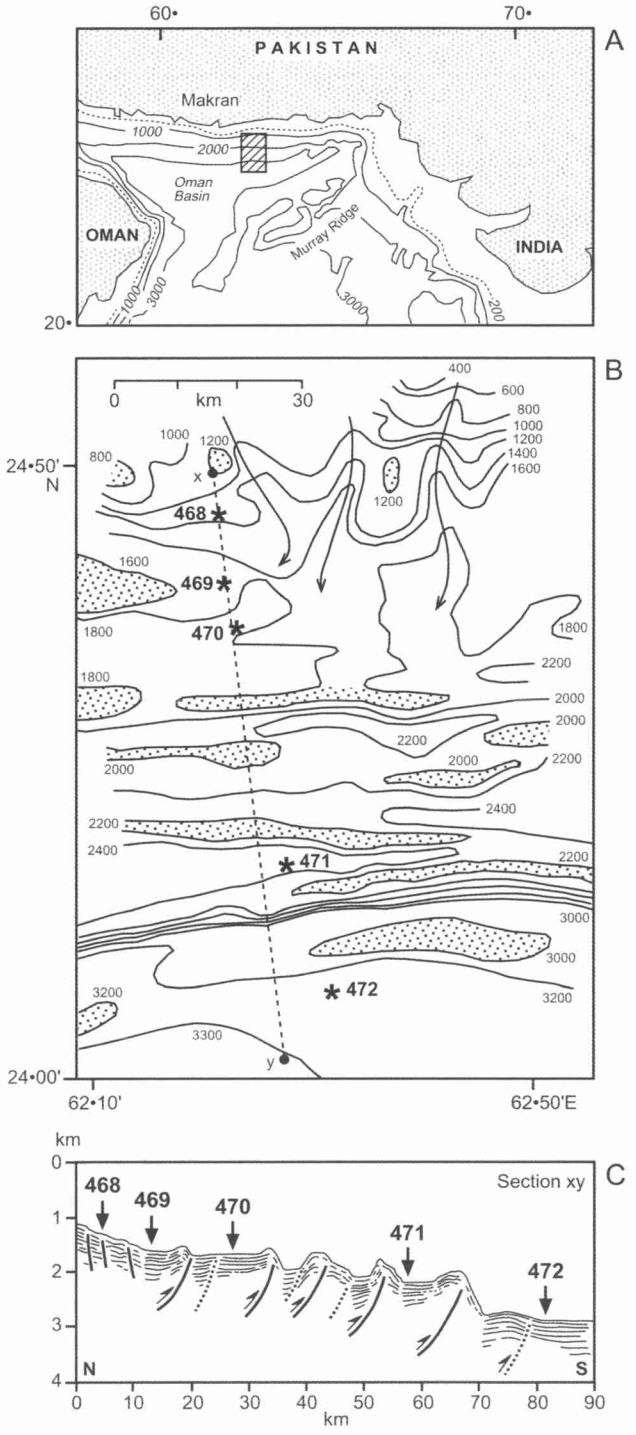

Fig. 1. (**a**) Location map, (**b**) detailed bathymetric map with core locations and (**c**) summary bathymetric profile of slope transect along which cores were positioned.

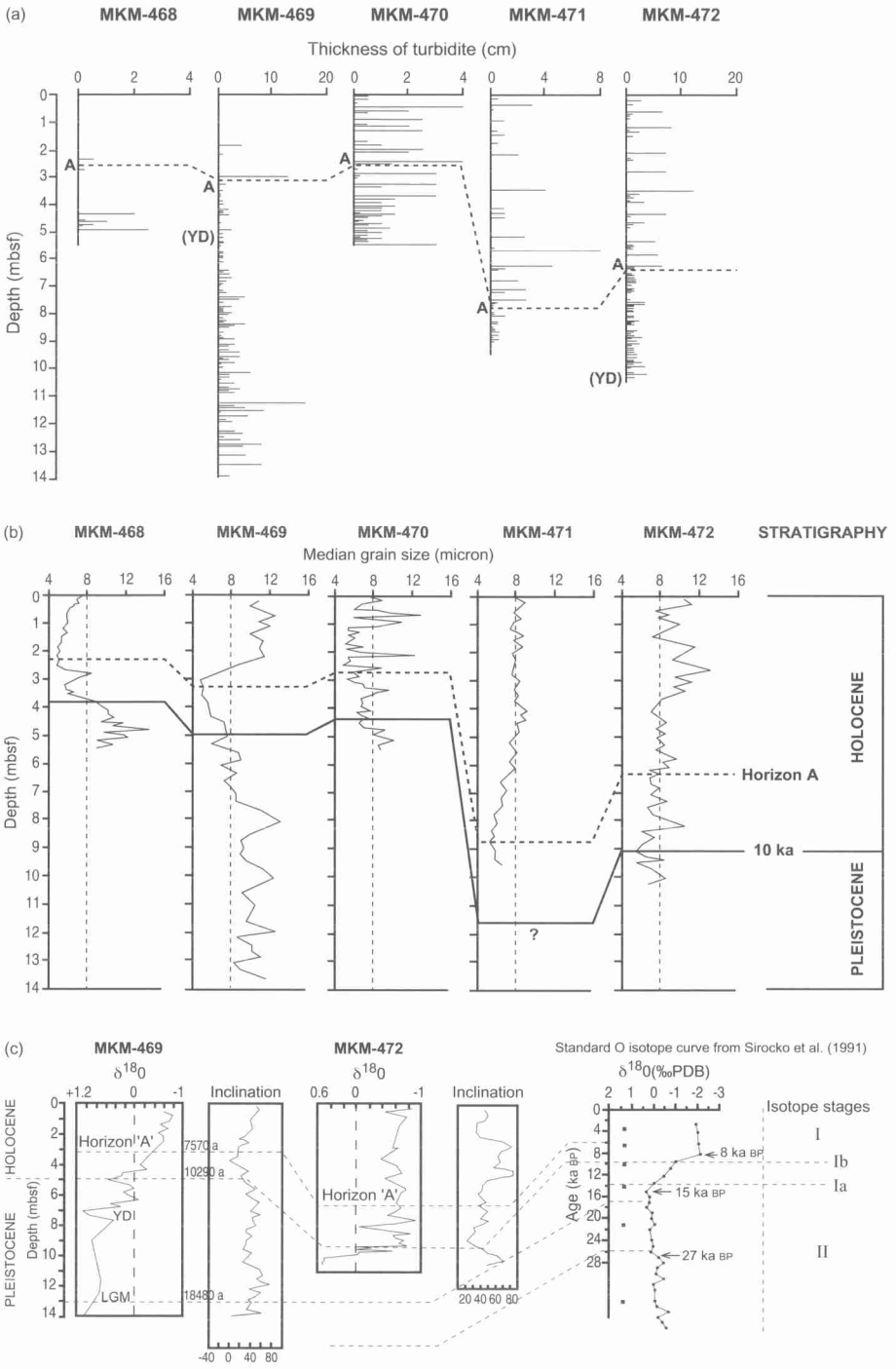

Fig. 2. Stratigraphic framework and correlation between cores. (**a**) Lithostratigraphic correlation for all five cores based on turbidite bed thickness and number. (**b**) Lithostratigraphic correlation for all five cores based on median grain size of hemipelagites. (**c**) Stratigraphic interpretation of oxygen isotope and magnetostratigraphic data from the two long cores (469 and 472). Comparison is made with the standard regional oxygen isotope curve of Sirocko *et al.* (1991). Figures shown in parentheses are AMS ^{14}C dates from Prins & Postma (2000).

higher ^{18}O values at about 13 m depth in core 469 may correspond to the last glacial maximum (LGM) at around 18 ka BP. By contrast, most of core 472 has ^{18}O values typical of the Holocene period, with Termination I occurring at 9–9.5 m depth.

The natural remanent magnetization (NRM) of 59 specimens from core MKM-469 and 40 specimens from MKM-472 were measured on a 2G cryogenic magnetometer. All specimens were subjected to stepwise demagnetization to a maximum field value of 40 mT. Bulk magnetic susceptibility measurements were made with a Bartington meter. For both cores, NRM values mainly vary between 10°and 45° (Fig. 2c) as would be expected for the present normal magnetozone at that latitude. A minor palaeomagnetic excursion is evident at 3.7 m in core 469 and 7.0 m in core 472. Although previously unrecognized in this area, we interpret this as a true low-latitude geomagnetic excursion (Tabrez 1995). An older possible reversal is just apparent at the base of core 469 (13.9 m depth). Using the oxygen isotope stratigraphy established above, the latest excursion is dated to occur between 6 and 8 ka BP, whereas the earlier one would be between 18 and 20 ka BP. This age is similar to the high-latitude excursions reported from Imuruk Lake (17–18 ka BP, Noltimer & Colvinaux 1976), and Baffin Bay (18 ka BP, Thouveny 1988), but probably not as old as the Mono Lake event between 24 and 9 ka BP (Denham & Cox 1971; Denham 1974; Liddicoat & Coe 1979), as we had previously thought.

Rates of sedimentation

On the basis of the stratigraphy outlined above, average sedimentation rates can be calculated for the various sites. For the Holocene period, these vary between about 0.38 m ka^{-1} (core 468) and 0.9 m ka^{-1} (core 472). The base of the Holocene sequence is probably not reached in core 471, but the estimated rate at this site for the latter part of the Holocene period is in excess of 1.4 m ka^{-1}. These values are an average for both turbidites and hemipelagites in the time period represented by each core. They are slightly higher than those found by Hutchison *et al.* (1981) (0.25–0.40 m ka^{-1}) for the Oman Abyssal Plain and 0.50 m ka^{-1} for the central basin of the Gulf of Oman (Stoffers & Ross 1979). For the slightly longer record recovered by core 469, the rate of sedimentation has decreased from *c.* 0.9 m ka^{-1} during late Pleistocene time to *c.* 0.5 m ka^{-1} for the Holocene period. These are very close to the rates of 0.41–1.1 m ka^{-1} reported by Wiedicke *et al.* (2001). Counting the number of discrete turbidites at each site yields a frequency of one event every 180–300 a.

Much higher rates of sedimentation during late Holocene time (2.3 m ka^{-1} SW of Ormara) are found further east along the upper slope within the oxygen-minimum zone, based on varve counts and ^{14}C data (von Rad *et al.* 1999*a*). In another upper slope core, directly off the Hingol River mouth, the turbidite-dominated succession accumulated at rates of 3–4 m ka^{-1}, and with an event frequency of up to 12 per century (von Rad *et al.* 1999*a*, *b*, and pers. comm. 2001).

Sediment facies

Facies characteristics and distribution

In the five piston cores recovered, turbidites and hemipelagites are seen to be closely interbedded, although with relatively more turbidites in the ponded basin areas and more hemipelagites on the open slope. This distribution is confirmed by study of 3.5 kHz profiles, which show transparent drapesheet echofacies (Type A; hemipelagites) most common over the open slope and interbasinal highs, and strong parallel–multiple echofacies (Type D; turbidites) within the basins and on the abyssal plain. Basin margins and the steep flanks of interbasinal highs are characterized by irregular–chaotic echofacies (Type C; slumps and debrites). These echofacies types and interpretations follow Tabrez (1995). The relative proportions of the various facies at the core sites is given in Table 1.

The turbidites are dominantly fine grained, comprising mainly clay- and silt-grade muds, in

Table 1. *Relative proportion (in percentages) of different facies at each of the core sites*

Facies %	MKM-468	MKM-469	MKM-470	MKM-471	MKM-472
Turbidite	40	65	60	40	45
Hemipelagite	60	35	40	60	40
(Hemiturbidite)	(7)	(1–2)	(1–2)	(8)	(1–2)
Pelagite	0	0	0	0	15

The percentage of probable hemiturbidites is included in the overall value for hemipelagites, and also indicated separately in parentheses.

some cases with thin silts or silty sands at the base of beds. These coarse-grained intervals are typically 1–2 cm thick, and more rarely up to a maximum of 16 cm. The colour of the turbidites ranges from dark grey to blackish, becoming paler upwards and with a sharp colour change to pale green–greyish yellow in the upper part of the bed. The clay fraction of all turbidites examined is dominated by illite and chlorite, and the silt–sand fraction by quartz. Minor components include other clay minerals, feldspar, calcite and dolomite. Biogenic material is rare and organic carbon averages <0.6%. Compositional data have been presented fully by Tabrez (1995). The distribution of turbidite beds varies from core to core.

In some cases, particularly for cores 468 and 471, there are thick bioturbated units overlying the turbidites, but having a more turbiditic (terrigenous, darker colour) than hemipelagic (biogenic-rich, paler colour) nature in terms of colour and composition. These facies are probably equivalent to the hemiturbidites described by Stow & Wetzel (1990) from the distal Bengal Fan.

True hemipelagic units can be clearly distinguished from the intervening turbidites on the basis of texture, composition, sedimentary structures and colour. They comprise a foraminiferal and nannofossil biogenic fraction, and terrigenous silty clays of similar composition to the turbidites described above. They appear to be fully homogenized and mottled by bioturbation, although distinct burrow traces are not very common. The colour varies from olive grey to pale grey. The upper part of hemipelagic units is typically rich in foraminifers and nannofossils, with indistinct bioturbation. The lower contact with the underlying turbidite is usually gradational whereas the contact with the overlying turbidite is sharp. All hemipelagites are very poorly sorted, typically showing weakly developed bimodal or polymodal peaks on grain-size distribution curves. Bed thicknesses range from 5 to 50 cm.

Pelagic facies are recognized only in certain specific horizons in core 472 (forming 10–15% of the recovered core). They occur as thin to thick beds (10–40 cm), typically located towards the top of a hemipelagic unit. They have a completely gradational contact with the underlying hemipelagite and are distinguished from the latter on the basis of their paler colour and higher percentage of pelagic biogenic material (foraminifers and nannofossils). The terrigenous content is <25%, including traces of clays and fine quartz.

Bed thickness and vertical sequences

Thin-bedded, fine-grained turbidites are very common in all slope-apron, lower fan and basin plain environments, both modern and ancient, and yet many of their attributes are still poorly known. For example, small-scale cycles (<10 m) of bed thickness variation in such turbidite successions have been recognized but are little understood (Piper & Stow 1991; Hiscott *et al.* 1992; Forster 1995). Such variation is evident from visual inspection of Makran margin cores, in which we note both thinning-upwards and thickening-upwards sequences over a few metres of section. However, there is much discussion on the validity of sequences noted that are based solely on visual investigation of the core or outcrop and hence are liable to subjective bias introduced by preconceptions, plotting methods and so on (Hiscott 1981; Hiscott *et al.* 1992). Certain statistical procedures can therefore help provide a more objective assessment of sequences and their nature (Weedon 1985, 1989).

For this study we have examined both bed thickness and the sequence of bed thickness variation in Makran margin cores. Only the basal silt–sand layers of turbidites were measured, where these were in excess of 0.5 cm thick. The overlying muddy parts of the turbidite beds were ignored, partly because of the difficulty in determining the boundary between turbidite and hemipelagite, and partly because the mud thickness (2–20 cm) generally correlated closely with the sand thickness. The data were analysed using the time series autocorrelation and runs tests (Davis 1973; Forster 1995).

The bed thickness data are shown in Table 2. In general, very thin beds (<3 cm) are dominant. Cores 468, 470 and 471 show the greatest number of 0.5 cm thick beds, followed by 1 and 2 cm beds, core 472 shows equal numbers of 0.5 and 1 cm beds, whereas core 469 has equal numbers of 1 and 2 cm beds. When plotted on a cumulative frequency logarithmic plot (Fig. 3) of the number $N(t)$ of turbidite beds with a thickness $>t$ v. t, in the same way as carried out by Hiscott *et al.* (1992) and Forster 1995 for volcaniclastic turbidites from the Izu–Bonin forearc basin, the data approximate to a power-law distribution in which $N(t)$ is proportional to tb, where b is a positive constant, as has been proposed for turbidite bed thickness by Hsu (1983). The best-fit slope for these data over bed thicknesses from 10 to 3 cm is slightly >1.0, as found by Hiscott *et al.* (1992), although the decrease in slope at the thinner end of the spectrum is more marked than found previously. The data also show a relatively good fit for a log-normal distribution, and for some sites this appears to be a better fit than the power-law distribution.

The small-scale trends of bed thickness variation observed by visual inspection of the cores are

Table 2. *Data for turbidite bed thicknesses (silt–sand bases only) at each core site*

Thickness of sand–silt base (cm)	Number of beds				
	MKM-468	MKM-469	MKM-470	MKM-471	MKM-472
0.5	12	35	24	26	30
1	4	36	12	16	23
2	1	32	11	3	4
3	1	10	1	1	8
4	–	4	1	1	–
5	–	5	1	–	1
6	–	1	1	–	1
7	–	–	–	–	4
8	–	3	–	–	–
12	–	–	–	–	–
13	–	1	–	–	1
16	–	1	–	–	–
Total	18	128	61	47	72

not evident in any of the statistical tests applied (e.g. runs test), which is similar to the result found by Forster (1995). However, results of the autocorrelation study do show some cyclicity, with the most significant cycles occurring at three-bed and 10-bed intervals for core 469, at five-bed intervals for cores 470 and 471, and at six-bed intervals for core 472. The three- and six-bed cycles are significant at the 95% confidence level; the others are close to the 95% level. Other lags are not significant. Selected autocorrelation correlograms are shown in Fig. 4.

Several significant observations and interpretations can be made as follows:

(1) Thin-bedded, fine-grained turbidites are typical of the Makran slope, and are commonly arranged in small-scale (<10 m) vertical sequences of thinning or thickening upwards. These are probably caused by a mechanism analogous to that for lobe progradation and migration on submarine fans. The lack of statistical validation of these sequences is partly due to the unsatisfactory nature of the tests themselves (Forster 1995).

(2) The power-law distribution of bed thickness observed implies a large number of thin beds and small number of thick beds, as might be expected either from frequent seismic triggering of turbidity current events on an active margin (Hiscott *et al.* 1992), or from frequent river flood events. Either mechanism coupled with relatively short transport pathways to small basin plains will favour the deposition of fine- and medium-bedded turbidites, and hence a log-normal distribution of bed thickness.

(3) The very small-scale cycles noted by autocorrelation (3–6 beds) are probably best interpreted as compensation cycles (Mutti & Sonnino 1981; Forster 1995), in which the depositional relief of each turbidite deposited subtly affects the flow pathway and depositional locus of the subsequent event.

Sedimentary structures and sequence

Fine-grained turbidites show a distinctive suite of structures not seen in the classical (medium-grained) turbidites characterized by the Bouma sequence (Piper & Stow 1991; Stow *et al.* 1996). Piper (1978) first refined the scheme of Bouma (1962) to cover sedimentary features noted in turbidite muds, by dividing the E division into E1, E2 and E3. Stow (1977) further recognized nine structural divisions in fine-grained silt–mud turbidites, which he termed T0–T8 (Stow & Shanmugam 1980) (Fig. 5). The complete set of structures T0–T8 is rarely present in a single bed although the order of the sequence is believed to be correct (e.g. van Weering & van Iperen 1984; Lash 1988). However, the study by Porebski *et al.* (1991) is the first and, to our knowledge, the only one to have applied Markov chain analysis to transitions between the T0–T8 divisions to statistically verify their order of occurrence.

The Makran margin turbidites have been described in great detail, both visually and by X-radiographs, and so provide a good opportunity to further examine the Stow sequence. About 200 fine-grained turbidites have been examined in detail and their structural divisions carefully logged. All the T0–T8 divisions have been recognized, though very rarely as a complete sequence. The order of these structural divisions was studied using Markov chain analysis techniques (see Lindholm (1987) and Tucker (1988) for the full method). The raw data consist of an observed number of upward transitions, which are plotted in

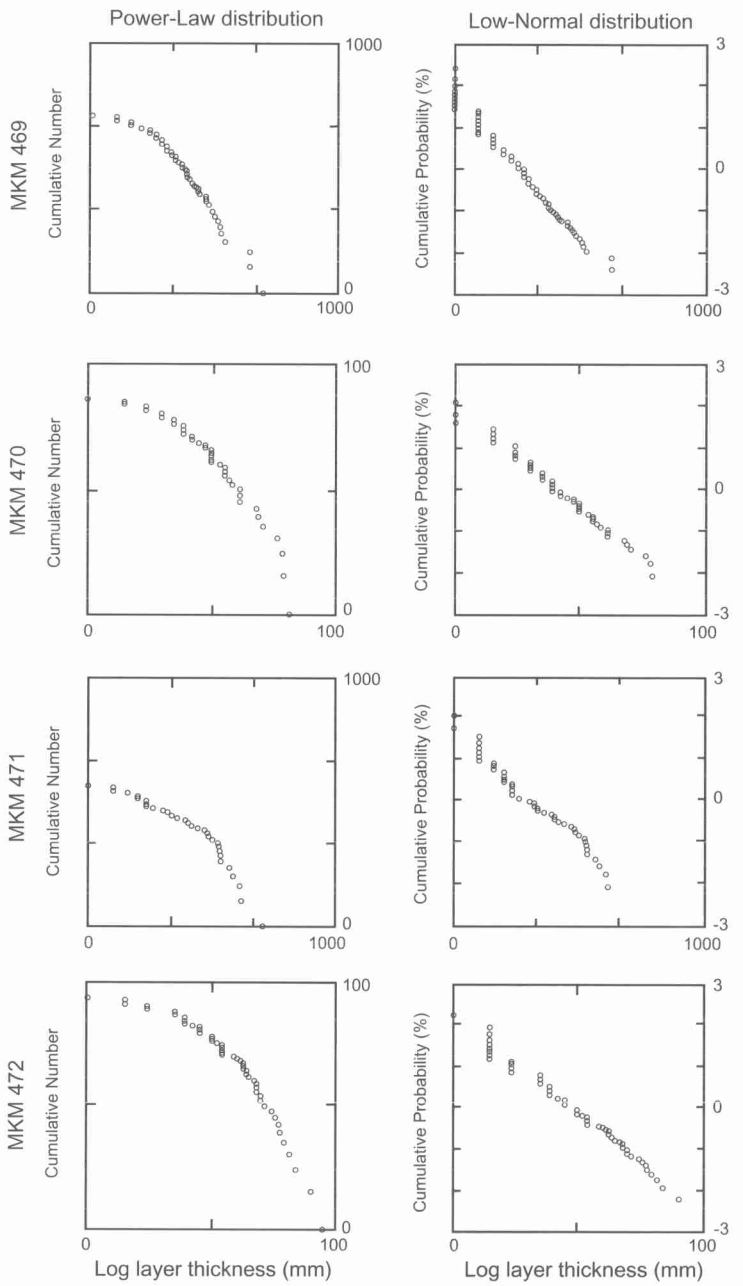

Fig. 3. Cumulative frequency plots for turbidite bed thickness for four of the five sites. Data are plotted to show best fits for both power-law and log-normal distributions. It should be noted that the scales for the different plots are necessarily varied to fit into the same figure.

matrix form. This tally matrix is converted to transition probabilities by dividing the number of transitions in each cell by the total number of transitions for the row containing the cell (row total) in the tally matrix. The difference matrix then derived shows the observed minus the calculated random probabilities with a range of values from -1.0 to $+1.0$. Positive values indicate transi-

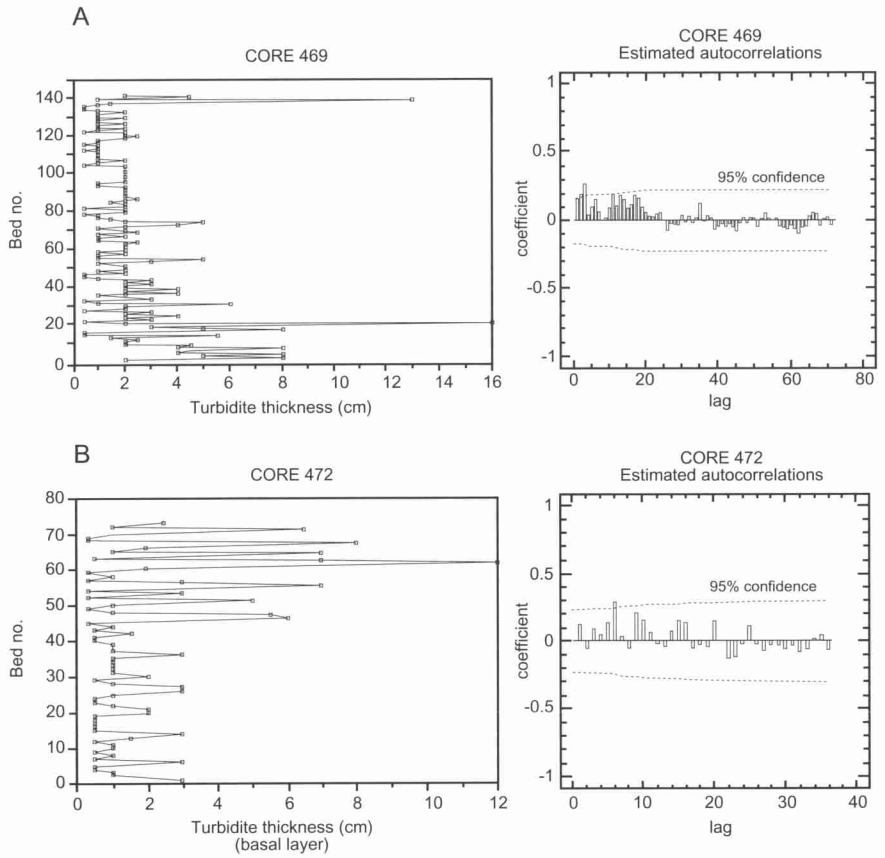

Fig. 4. Turbidite bed thickness data from selected sites. (**a**) Turbidite bed thickness for core 469 together with autocorrelation correlogram for these data. Dashed lines show the 95% confidence limit. (**b**) Turbidite bed thickness for core 472, together with autocorrelation correlogram for these data. Dashed lines show the 95% confidence limit.

tions more frequent than random, significantly so where the value is $>+0.1$, whereas negative values are taken as indicative of random transitions.

Results of this Markov chain analysis for all cores combined are given in Table 3 and illustrated in a facies relationship diagram (Fig. 6), which summarizes the principal transitions between turbidite divisions, and indicates both their frequency and direction. Several very interesting features are apparent:

(1) The most common transitions are those to the upper right of the diagonal, and the single most common transition from each division is to that immediately overlying it in the Stow (1977) sequence. T0–T2 is the only exception to this standard order, suggesting that the T1 division is either not very common or not so readily recognized.

(2) The transition from any of the divisions to T0 is also relatively common. These are taken as representing top-cut-out sequences capped by a new T0 basal division. Minor numbers of 'reverse' transitions to T3 and T4 can also be taken as top-cut-out sequences.

(3) Hemipelagites (HP) can show transitions back to any of the turbidite divisions, although T0 and T3 are the most common basal divisions observed (126 and 98 occurrences, respectively). The transition from any of the divisions to HP is also common.

(4) In most cases, the transitions that are common numerically also have a relatively high positive difference value, which is often highly significant ($>+0.2$). It is these difference values, rather than the actual numbers of transitions, that are used to construct the facies relationship diagram (Fig. 6). This demonstrates clearly that the

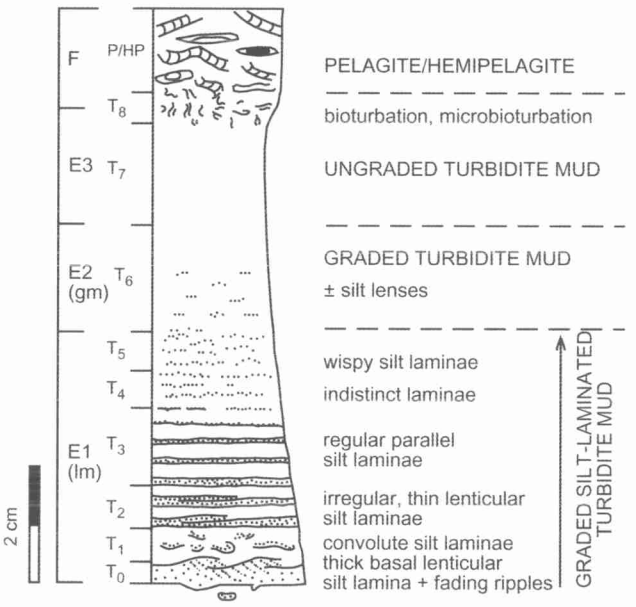

Fig. 5. Standard sequence of structures in fine-grained turbidites (after Stow 1977; Stow & Shanmugam 1980). The T0–T8 divisions are compared with the E1–3 divisions of Piper (1978) and the lm and gm divisions of Einsele (1991).

dominant transitions are all in the order predicted by the Stow sequence.

When the data for individual cores are considered separately (see Tabrez 1995), and also from visual inspection, it is clear that important differences exist between sites. The most common basal divisions vary from one site to another, and different numbers of base-cut-out, mid-cut-out and top-cut-out sequences are present. To characterize these differences, a Proximality Index for fine-grained turbidites (PI_{fgs}) has been devised, analogous to that for medium-grained turbidites that show Bouma sequences (Walker 1984). This index is given by the formula

$$PI_{fgs} = (T_{0123}/T) \times 100\%$$

where T_{0123} is the number of beds beginning with T0, T1, T2 or T3 divisions and T is the total number of beds. When applied to the Makran margin sites, this gives: core 468, 16%; core 469, 42%; core 470, 41%; core 471, 41%; core 472, 52%.

Although it is the most upslope, the location of core 468 is apparently less 'proximal', presumably because it is bypassed by turbidity currents. Conversely, the most distal site, for core 472 on the abyssal plain, has the highest Proximality Index. This is either because the larger turbidity currents deposit their load only when they reach the basin plain and/or because there is a separate input of turbidity currents deflected from the slope region further east, which is cut by more major submarine channels (Kukowski *et al.* 2001).

Sediment grain size

For this study grain size has been measured using a Malvern 2600 Particle Analyzer with a 100 mm focal length. This configuration provided measurements in 32 discrete size intervals between 0.5 and 188 μm (equivalent volume diameter). Some 300 samples were taken from hemipelagic facies at all sites (5–20 cm intervals), and 65 samples from all distinctive turbidites in the two longer, turbidite-dominated cores 469 and 472. Results have been computer plotted and moment statistics determined including median, mean, standard deviation and skewness.

The median grain size of all hemipelagite samples analysed varies between about 5 and 15 μm, and most of these samples lie between the tighter range of 5–10 μm. The mean size values tend to be slightly higher, typically 7–16 μm, and ranging to 27 μm. Sorting is generally very poor. Most samples show slight to moderate positive skewness. Three shapes of grain-size distribution curves can be recognized: very fine unimodal, fine bimodal and coarser polymodal (Fig. 7).

The vertical variation of grain size for hemipelagites analysed throughout the cored intervals

Table 3. *Markovian tally matrix for 651 observed transitions between turbidite divisions (T0–T8) and hemipelagite units (HP)*

	T0	T1	T2	T3	T4	T5	T6	T7	T8	HP	Total
T0		15	19	17	2	5	18	1	6	43	126
		0.12	0.15	0.13	0.02	0.04	0.14	0.01	0.05	0.34	
		0.08	0.09	0.08	−0.03	0	0.08	−0.04	0.02	0.29	
T1			7	4	1	1	2		1	4	20
			0.35	0.20	0.05	0.05	0.10	–	0.05	0.20	
			0.29	0.09	0.01	0.01	0.02		0.01	0.09	
T2	2	–		17	4	1	4	1	–	5	34
	0.06			0.50	0.12	0.03	0.12	0.03		0.15	
	0.02			0.34	0.06	−0.01	0.06	−0.01		0.10	
T3	6	1	3		46	2	7	2	3	28	98
	60.06	0.01	0.03		0.46	0.02	0.07	0.02	0.03	0.26	
	0.04	−0.03	−0.03		0.36	−0.02	0.05	−0.03	−0.04	0.21	
T4	8	–	1	11		11	8	–	5	13	57
	0.14		0.02	0.19		0.19	0.14		0.09	0.23	
	0.10		−0.08	0.15		0.15	0.10		0.02	0.20	
T5	4	–	–	–	–		15	–	–	4	23
	0.17						0.65			0.17	
	0.08						0.56			−0.08	
T6	14	–	2	7	2	2		21	12	14	74
	0.19		0.03	0.09	0.03	0.03		0.28	0.16	0.19	
	0.12		−0.01	0.07	−0.01	−0.01		0.23	0.10	0.12	
T7	5	1	–	2	–	–	–		14	9	31
	0.16	0.03		0.06					0.45	0.29	
	0.08	−0.01		0.01					0.38	0.14	
T8	14	–	–	4	–	–	1	–		33	52
	0.27			0.08			0.02			0.63	
	0.18			0.06			−0.07			0.38	
HP	69	2	8	36	3	3	7	2	6		136
	0.51	0.01	0.06	0.26	0.020	0.02	0.05	0.01	0.04		
	0.38	−0.02	0.06	0.16	.02	0.02	0.04	−0.02	0.03		
	122	19	40	98	58	25	62	27	47	153	651/651

It should be noted that the top row of values for each division shows the actual number of observed transitions. The middle row is the observed probability. The bottom row shows the difference between the observed and random probabilities and is taken as a measure of the statistical significance of a particular transition. Positive values suggest ordered and negative values random transitions; a value of $> +0.1$ is taken as a significant ordered transition.

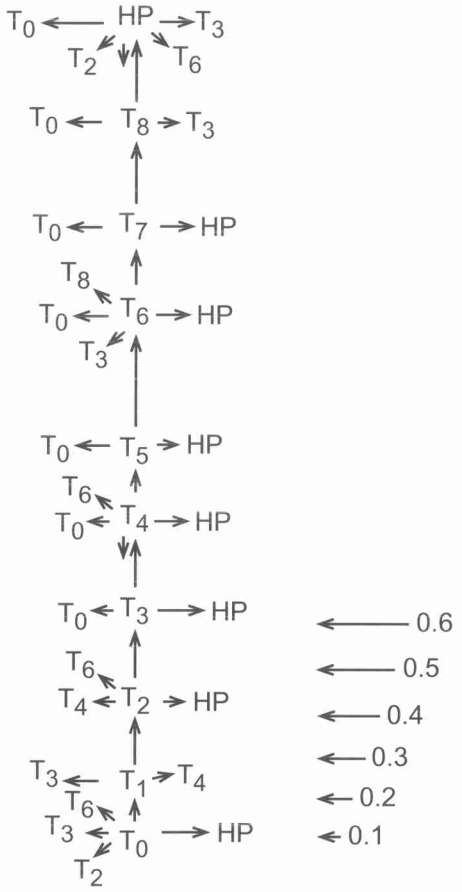

Fig. 6. Facies relationship flow diagram based on the Markovian difference matrix for 651 observed vertical transitions between turbidite divisions (T0–T8) and hemipelagite units (HP). The relative lengths of the arrows indicate the relative probabilities of the various transitions, rather than the actual numbers of transitions. The dominance of the standard sequence, and the presence of partial sequences showing the standard direction of transitions, should be noted.

at each site is extremely interesting. First, there is a zone of minimum grain size at between 2 and 3 m depth in cores 468, 469 and 470, and between 7 and 10 m in cores 471 and 472. This has been used in our lithostratigraphic correlation between cores (see above, Fig. 2a). Second, there is a small-scale oscillation or cyclicity of median grain size evident over a vertical distant of 0.2–1.0 m. This oscillation is particularly marked, with variation in median grain size of 4–6 μm, only at certain horizons in each of the cores.

Grain-size characteristics for the turbidites analysed from cores 469 and 472 are very different from those of the hemipelagites described above. Where an individual turbidite has been analysed in detail (i.e. three or more samples), there is evidence of a clear gradation in properties from base to top. One relatively thick (30 cm) silt-laminated turbidite from core 472 is illustrated in Fig. 8. The nine separate analyses show a change from base to top in median grain size (from 34.8 to 6.3 μm), mean grain size (from 37.1 to 8.7 μm), sorting (from 7.8 to 26.5 μm), and skewness (from unity to 2.5). The shape of the grain-size distribution curves change from a distinctly peaked, well-sorted curve with a marked fine tail (positive skewness) at the base, to a broad somewhat irregular curve at the top. Similar characteristics are observed throughout, although the basal silt–sand layers are slightly coarser in core 469 (mean 20–70 μm, median 12–56 μm), than in core 472 (mean 12–64 μm, median 9–57 μm). The shapes of the grain-size distribution curves range from sharply peaked, well-sorted with a small fine tail for the coarser layers, to broadly domed, irregular, poorly sorted and with a very large fine tail for the finer layers.

In summary, we recognize and interpret the following features for Makran margin hemipelagites:

(1) The grain-size characteristics are similar to those of mixed biogenic–clastic hemipelagites reported in previous work, and are taken as typical for a terrigenous fluvial–aeolian source (Stow & Tabrez 1998). Fluvial input is probably dominant in this case (von Rad, pers. comm. 2001).

(2) The unimodal distribution reflects an input of nannofossils and fine clays only, the latter probably from fluvial suspension; the bimodal distribution reflects an input of nannofossils together with mixed terrigenous material of aeolian and fluvial derivation; and the polymodal distribution is caused by a heterogeneous input of nannofossils and foraminifers, and terrigenous mud, silt and fine sand of mixed source, particularly with a greater influence of direct fluvial input at lowered sea level.

(3) The vertical variation of median grain sizes over the length of the cores can be interpreted in terms of climatic and sea-level controls: the coarser grain size at depth reflects sea-level lowstand during the last glacial period and a multi-sourced input; the mid-core grain-size low reflects sea-level rise and a fining of the fluvial input from early to mid-Holocene time; and the subsequent grain-size increase may then reflect increased aeolian input as a result of onshore aridification.

(4) The vertical oscillation of grain size over 0.2–1.0 m has a time scale of about 500–1000 a and probably reflects slight climatic variation of this order, which in turn influences aeolian–fluvial input and/or biogenic productivity.

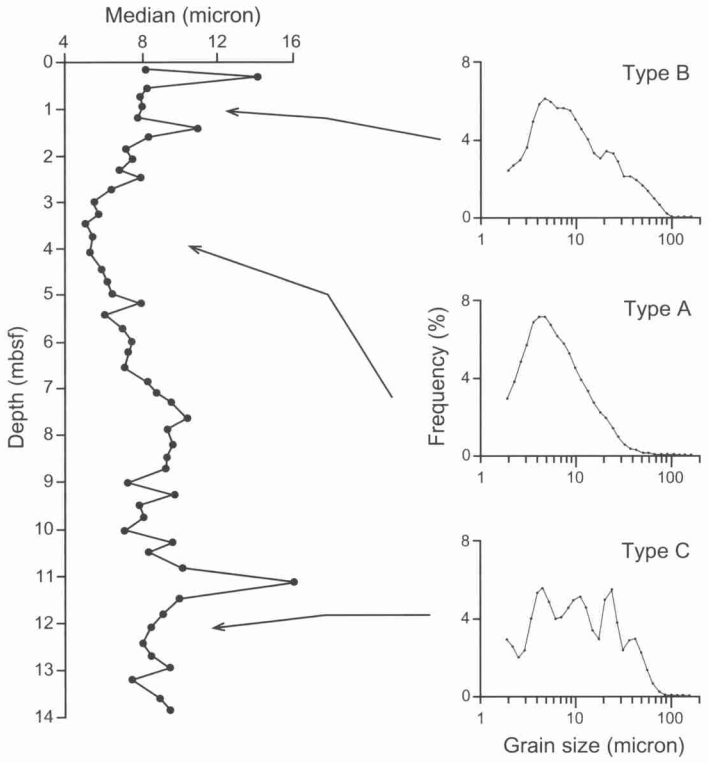

Fig. 7. Typical grain-size distribution curves for selected hemipelagite facies from core 469. Type A, very fine, unimodal; Type B, fine, bimodal; Type C, mixed, poorly sorted, polymodal. The median size plot is based on carbonate-free samples, whereas the grain-size distribution curves include the carbonate fraction.

(5) The lack of any clear-cut onshore–offshore trend in grain size is in part due to the morphological complexity of margin, and hemipelagic dispersion that generally follows the turbidite pathways, and in part due to the multi-sourced composition.

For the fine-grained turbidites, the following points can be made:

(1) The grain-size characteristics of the Makran margin turbidites are very typical of those of fine-grained turbidites elsewhere (e.g. Piper & Stow 1991; Stow *et al.* 1996) and very different from those of the hemipelagites. The upward change through a single graded, laminated unit is also typical.

(2) There is a relatively clear offshore decrease in grain size from core 469 to 472, reflecting the downslope distribution pathway, but apparently not coincident with the inverse nature of the proximality index between these sites, as noted above.

(3) There is no clear relationship between grain size and bed thickness for the measured turbidites.

Discussion

Turbidite statistics

Makran margin sedimentation is characterized by a relative abundance of fine-grained turbidites, approximately one event per 180–300 a. Careful study therefore allows a more rigorous or semi-quantitative analysis of turbidite features than is normally possible.

Statistical analysis of bed thickness data shows best-fit lines with either an imperfect power-law distribution or a log-normal distribution. Whereas Hiscott *et al.* (1992) argued that a power-law distribution should be expected for turbidite successions because of the likely scale-invariance of the (seismic) triggering mechanism, Forster (1995) demonstrated that both log-normal and power-law distributions are present in different turbidite successions and concluded that the former are the result of various external effects on the transport and deposition by turbidity flows subsequent to their initiation. In the case of the Makran turbidites, it may be that the local morphology of

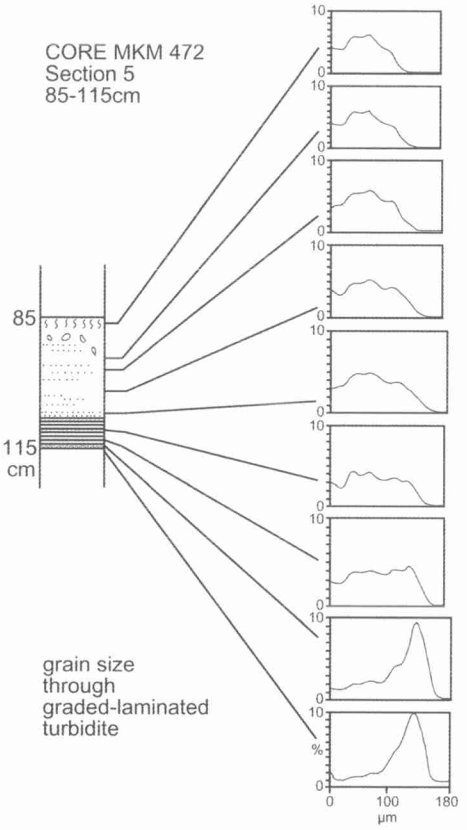

Fig. 8. Series of samples taken through a silt-laminated mud turbidite of core 472, showing typical grain-size distribution curves (whole fraction) from base to top of the bed.

partly interconnected slope basins is sufficiently uniform that it favours the relatively narrow range of turbidite thicknesses shown by the log-normal distribution. Alternatively, the frequency of seismic or river flood trigger events coupled with a steady input of sediment to the shelf–upper-slope source area, might favour a particular range of flow dimensions and hence turbidite thicknesses.

Bed thickness variation observed using an autocorrelation statistical technique reveals some small-scale cyclicity (3–6 beds), which can most readily be interpreted as the result of compensation cycles forming in the small basin settings (Mutti & Sonnino 1981). The main mechanism for their development is lateral shifts in the site of turbidity current deposition as a result of the microtopography created by previous deposits. We would also agree with the findings of Forster (1995), from other turbidite series, that the variation is cyclic and typically symmetrical, rather than repeatedly thickening upwards as originally proposed by Mutti & Sonnino (1981).

Markov chain analysis has allowed an objective assessment of the sequence of structures found in fine-grained turbidites, thereby testing the validity of the standard model proposed by Stow (1977) and Stow & Shanmugam (1980). On the basis of data from 651 transitions between divisions, the order of the Stow sequence (T0–T8) is found to be fully valid for over 95% of the transitions. This supports an earlier testing of the sequence by Porebski *et al.* (1991) in turbidites from the Zaire Fan.

Furthermore, partial sequences of all turbidites are the norm, with mid-cut-out sequences being most common and base-cut-out sequences second in importance. The latter might be expected of relatively 'distal' turbidites across a slope showing a distinct lack of channelization. The absence of the middle divisions may reflect relatively rapidly deposition (at least of the upper divisions) from a partially ponded turbidity current on entering the slope basins. However, the presence of well-defined silt laminae (T0 and T3–T4 divisions especially) implies relatively mature turbidity currents and sufficiently slow deposition (at least of the basal divisions) to allow depositional sorting through the boundary layer (Stow & Bowen 1980). A Proximality Index for fine-grained turbidites (see Walker (1967, 1984) for medium-grained turbidites) has been found useful for characterizing suites of turbidites from different sites.

In a very few of the turbidites studied, non-standard sequences or repetition of certain divisions were noted. These could be explained by either (1) reflected and reversed flows in ponded basins, or (2) a multiple flow mechanism.

Sediment source, distribution and controls

There are several potential sources of terrigenous material for turbidite and hemipelagite sedimentation on the Makran margin. These include: (1) local riverborne material from the Oman–Makran hinterland (e.g. Hub, Hingol and other rivers); (2) airborne material from arid regions of Pakistan and NW India; (3) airborne material from the Arabian–African deserts; (4) direct or indirect supply from the Indus River system.

In general, the results of clay and silt mineralogical analysis (see also Tabrez 1995) show a relatively uniform sediment composition of materials derived mainly from the north (i.e. (1) and (2) above). There is little evidence for a marked palygorskite–smectite clay mineral assemblage typical of the Arabian–African desert source, and also little possibility for much Indus-derived material to find its way onto the Makran slope. The

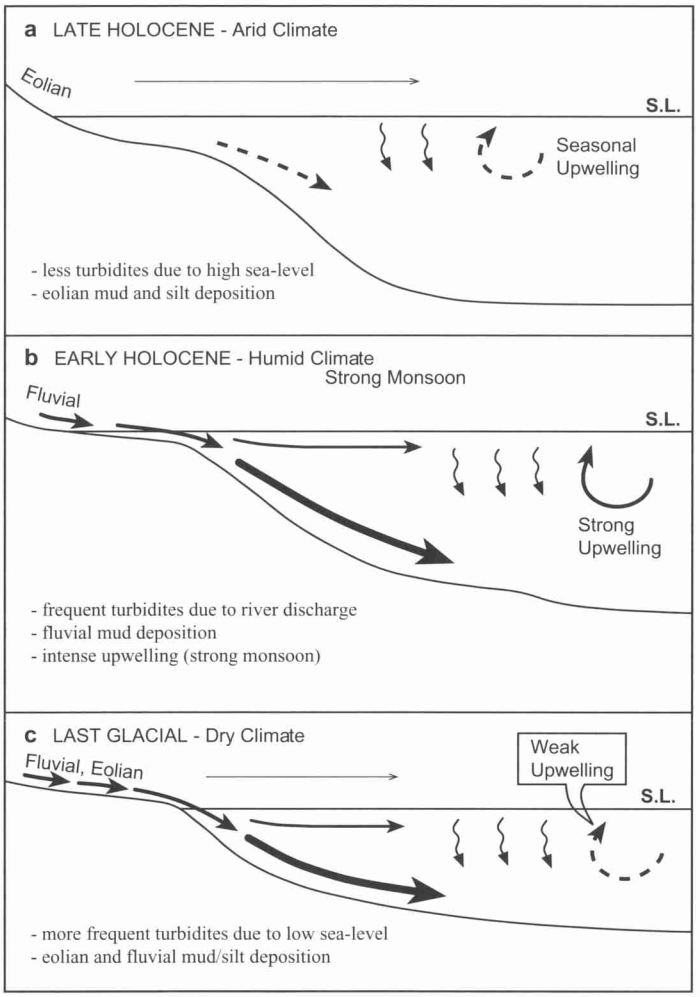

Fig. 9. Principal controls and sediment supply routes for the Makran margin during the last glacial, and early and late Holocene periods. This figure shows a schematic summary of controls; for a more detailed overview, see Prins *et al.* (2000*a, b*).

abyssal plain site for core 472 could, physiographically, have a more direct connection with an Indus source, but there is little mineralogical support for this.

Although distinct channels are incised into the steeper, upper part of the slope, turbidity current pathways rather than a true channel system can be observed across much of the rest of the study area (Fig. 1). Further east, however, channel development and incision has continued across the whole slope (Kukowski *et al.* 2001). Turbidity currents generated on the outer shelf to upper slope may initially be channelized, but then apparently follow a somewhat irregular and sinuous pathway that cuts through gaps in the fold ridges and flows either to the east or west through the semi-enclosed slope basins. Hemipelagic dispersion is believed to be affected and partly focused by the same distribution pathways. In some cases, hemiturbiditic sedimentation (Stow & Wetzel 1990) is recognized, perhaps resulting from the interaction of turbidity currents with the basin–ridge topography.

Tectonic activity, fluvial input, sea-level fluctuation and climate variation have all influenced sedimentation on the Makran margin during the time period represented in this study (Fig. 9), although their relative significance has varied and is not always easy to ascertain.

(1) During the last glacial period, sea level was lower and the climate relatively arid. Turbidite

input was frequent, and hemipelagic sedimentation was multi-sourced, with less direct fluvial discharge and more aeolian dispersion of terrigenous material, as well as a biogenic pelagic contribution. A similar interpretation for the region south of the Indus delta was presented by von Rad *et al.* (1999a).

(2) During deglaciation, sea level rose and the climate became more humid. Turbidite input remained frequent, although with a trend towards thinner beds evident in some of the cores, perhaps related to a retreat of the fluvial input points and fining of source material. Hemipelagic sedimentation was dominated by very fine-grained, distal, fluvial dispersions, perhaps partly as hyperpycnal discharge. A stronger monsoonal upwelling system developed, leading to primary biogenic input of mainly nannofossils.

(3) The post-glacial (late Holocene) period is one of sea-level highstand, and a climate that has resulted in generally increased aridity in the drainage basin. Von Rad *et al.* (1999*a*) carried out careful study of a piston core recovered from the upper slope off Karachi. They recognized cyclicity in varved sediments at decadal to centennial freqencies, which they related to climatic variability over the past 5 ka. Periods of higher precipitation and river discharge lead to thicker varves as well as more frequent turbidites. These alternate with more arid conditions, thinner varves and less frequent turbidites. With turbidite sedimentation much less frequent in our study area, the same degree of resolution is not possible. Hemipelagites are characterized by very fine-grained fluvial and aeolian input and pelagic supply of nannofossils under a more seasonal upwelling regime.

(4) The precise triggering mechanism for turbidity currents is always problematic. In the case of the Makran margin, turbidite thickness data from our study area indicate a relatively large number of events triggering frequent but small turbidity currents. This led to deposition of mainly thin- to medium-bedded turbidtes (<1 cm to 16 cm sandy divisions) with a frequency of one event every 200–300 a. However, we cannot distinguish between seismic activity or major river flood events as the principal trigger.

Much of the work for this paper was carried out by A.R.T. during tenure of a Pakistan Government Scholarship at the University of Southampton, and by M.A.P. as part of his Ph.D. research at Utrecht University, under the supervision of G. Postma. We also express our thanks to the National Institute of Oceanography, Pakistan, for encouraging the secondment of A.R.T. to undertake this project. The cores were collected as part of a joint Pakistan–Netherlands Indian Ocean Programme (NIOP) under the direction of W. J. M. van der Linden and C. H. van der Weijden. The Chief Scientist, officers and crew on board R.V. *Tyro* are thanked for their part in the success of this programme; as also are G. van der Linden, J. Stel and G. Postma at the University of Utrecht. We thank these individuals, in particular, for useful discussions and data exchange. We further acknowledge the excellent secretarial and technical support at our respective institutes, and a full and helpful review by U. von Rad.

References

ARTHURTON, R.S., FARAH, A. & AHMED, W. 1982. The Late Cretaceous–Cenozoic history of western Baluchistan, Pakistan—the northern margin of the Makran subduction complex. *In:* LEGGETT, J.K. (ed.) *Trench–Forearc Geology: Sedimention and Tectonics on Modern and Ancient Active Plate Margins*. Geological Society, London, Special Publications, **10**, 373–385.

BOUMA, A.H. 1962. *Sedimentology of some Flysch Deposits: a Graphic Approach to Facies Interpretation*. Elsevier, Amsterdam.

CLEMENS, S.C. & PRELL, W.L. 1990. Late Pleistocene variability of Arabian Sea summer monsoon winds and continental aridity: eolian records from the lithogenic component of deep-sea sediments. *Paleoceanography*, **5**, 109–145.

DAVIS, J.C. 1973. *Statistics and Data Analysis in Geology*. Wiley, New York, 232–235.

DENHAM, C.R. 1974. Counter-clockwise motion of paleomagnetic directions 24,000 years ago at Mono Lakes, California. *Journal of Geomagnetism and Geotectonics*, **26**, 487–498.

DENHAM, C.R. & COX, A. 1971. Evidence that the Laschamp polarity event did not occur 13,300–30,400 years ago. *Earth and Planetary Science Letters*, **13**, 181–190.

EINSELE, G. 1991. Submarine mass flow deposits and turbidites. *In:* EINSELE, G., RICKEN, W. & SEILACHER, A. (eds) *Cycles and events in stratigraphy*. Springer-Verlag, Berlin, 313–339.

FAUGERES, J.C. & GONTHIER, E. 1981. Les argiles de sédiments marins du Quaternaire récent dans le Golfe d'Aden et la Mer d'Oman. *Oceanologica Acta*, **4**, 4.

FORSTER, C. M., 1995. *The analysis of bed thickness trends in turbidite successions—a quantitative approach for the prediction of vertical sequences*. PhD thesis, University of Southampton.

HISCOTT, R.N. 1981. Deep-sea fan deposits in Macigno Formation (mid to upper Oligocene) Oligocene) of the Gordana valley, northern Apennines, Italy—discussion. *Journal of Sedimentary Petrology*, **51**, 1015–1021.

HISCOTT, R.N., COLELLA, A., PEZARD, P.A., LOVELL, M.A. & MALINVERNO, A. 1992. Sedimentology of deep-water volcaniclastics, Oligocene Izu–Bonin forearc Basin, based on Formation MicroScanner images. *In:* TAYLOR, B. & FUJIOKA, K. (eds) *Proceedings of the Ocean Drilling Program, Scientific Results, 126*. Ocean Drilling Program, College Station, TX, 75–94.

HSU, K.J. 1983. Actualistic catatrophism: address of the retiring President of the International Association of Sedimentologists. *Sedimentology*, 3–9.

HUTCHISON, I., LOUDEN, K.E. & WHITE, R.S. 1981. Heat flow and age of the Gulf of Oman. *Earth and Planetary Science Letters*, **56**, 256–262.

KOLLA, V., HENDERSON, L. & BISCAYE, P.E. 1976. Clay mineralogy and sedimentation in the western Indian Ocean. *Deep-Sea Research*, **23**, 949–961.

KOLLA, V., KOSTECKI, J.A., ROBINSON, F., BISCAYE, P.E. & RAY, P.K. 1981. Distribution and origin of clay-minerals and quartz in surface sediments of the Arabian Sea. *Journal of Sedimentary Petrology*, **51**, 563–569.

KOPP, C., FRUEHN, J., FLUEH, E.R., REICHERT, C., KUKOWSKI, N., BIALAS, J. & KELISCHEN, D. 2000. Structure of the Makran subduction zone from wide-angle and reflection seismic data. *Tectonophysics*, **329**, 171–191.

KUKOWSKI, N., SCHILLHORN, T., HUHN, K., VON RAD, U., HUSEN, S. & FLUEH, E.R. 2001. Morphotectonics and mechanics of the central Makran accretionary wedge off Pakistan. *Marine Geology*, **173**, 1–19.

LASH, G.G. 1988. Sedimentology and evolution of the Martinsburg Formation (Upper Ordovician) fine-grained turbidite depositional system, central Appalachians. *Sedimentology*, **35**, 429–447.

LIDDICOAT, J.C. & COE, R.S. 1979. Mono Lake geomagnetic excursion. *Journal of Geophysical Research*, **84**, 261–271.

LINDHOLM, R.C. 1987. *A Practical Approach to Sedimentology*. Allen & Unwin, London.

LUCKGE, A., DOOSE-ROLINSKI, H., KHAN, A.A., SCHULZ, H. & VON RAD, U. 2001. Monsoonal variation in the NE Arabian Sea during the past 5000 years: geochemical evidence from laminated sediments. *Palaeogeography, Palaeoclimatology, Palaeoecology*, **167**, 273–289.

MINSHULL, T.A. & WHITE, R.S. 1989. Sediment compaction and fluid migration in the Makran accretionary prism. *Journal of Geophysical Research*, **94**(B6), 7387–7402.

MUTTI, E. & SONNINO, M. 1981. Compensation cycles: a diagnostic feature of sandstone lobes. *IAS 2nd European Meeting, Abstract Volume*, 120–123.

NOLTIMER, R.M. & COLVINAUX, P.A. 1976. Geomagnetic excursion from Imuruk, Alaska. *Nature*, **259**, 197–200.

PIPER, D.J.W. 1978. Turbidite muds and silts on deep-sea fans and abyssal plains. *In:* STANLEY, D.J. & KELLING, G. (eds) *Sedimentation in Submarine Canyons, Fans, and Trenches*. Dowden, Hutchinson and Ross, Stroudsburg, PA, 163–176.

PIPER, D.J.W. & STOW, D.A.V. 1991. Fine-grained turbidites. *In:* EINSELE, G. & SEILACHER, A. (eds) *Cycles and Events in Stratigraphy, 2nd*. Springer, Berlin, 360–376.

POREBSKI, S.J., MEISCHNER, D. & CORLICH, K. 1991. Quaternary turbidites from South Shetland Trench, West Antarctica: recognition and implications for turbidite facies modelling. *Sedimentology*, **38**, 691–715.

PRELL, W.L. & STREETER, H.F. 1982. Temporal and spatial patterns of monsoonal upwelling along Arabia: a modern analogue for the interpretation of Quaternary SST anomalies. *Journal of Marine Research*, **40**, 143–155.

PRELL, W.L., NIITSUMA, N., *ET AL.* (eds) 1989. *Proceedings of the Ocean Drilling Program, Initial Reports, 117*. Ocean Drilling Program, College Station, TX.

PRELL, W.L. *ET AL.*1990. Neogene tectonics and sedimentation of the SE Oman continental margin: results from ODP Leg 117. *In:* ROBERTSON, A.H.F., SEARLE, M.P. & RIES, A.C. (eds) *The Geology and Tectonics of the Oman Region*. Geological Society, London, Special Publications, **49**, 745–758.

PRINS, M.A., 1999. *Pelagic, hemipelagic and turbidite sedimentation in the Arabian Sea during the late Quaternary*. PhD thesis, Utrecht University.

PRINS, M.A. & POSTMA, G. 2000. Effects of climate, sea level and tectonics unravelled for last deglaciation turbidite records of the Arabian Sea. *Geology*, **28**, 375–378.

PRINS, M.A., POSTMA, G., CLEVERINGA, J., CRAMP, A. & KENYON, N.H. 2000*a*. Control on terrigenous sediment supply to the Arabian Sea during the late Quaternary: the Indus Fan. *Marine Geology*, **169**, 327–349.

PRINS, M.A., POSTMA, G. & WELTJE, G.J. 2000*b*. Control on terrigenous sediment supply to the Arabian Sea during the late Quaternary: the Makran Continental Slope. *Marine Geology*, **169**, 351–371.

QUITTMEYER, R.C. & KAFKA, A.L. 1984. Constraints on plate motions in southern Pakistan and the northern Arabian Sea from the focal mechanisms of small earthquakes. *Journal of Geophysical Research*, **89**, 2444–2458.

REICHART, G.J. *ET AL.* 1997. A 225 ky record of dust supply, paleoproductivity and the oxygen minimum zone from the Murray Ridge (northern Arabian Sea). *Palaeogeography, Palaeoclimatology, Palaeoecology*, **134**, 149–169.

REICHART, G.J., LOURENS, L.J. & ZACHARIASSE, W.J. 1998. Temporal variability in the northern Arabian Sea oxygen minimum zone (OMZ) during the last 225,000 years. *Paleoceanography*, **13**, 607–621.

SCHULZ, H., VON RAD, U. & VON STACKELBERG, U. 1996. Laminated sediments from the oxygen minimum zone of the NE Arabian Sea. *In:* KEMP, A.E.S. (eds) *Paleoclimatology and Paleoceanography from Laminated Sediments*. Geological Society, London, Special Publications, **116**, 185–207.

SCHULZ, H., VON RAD, U. & ERLENKEUSER, H. 1998. Correlation between Arabian Sea and Greenland climate oscillations of the past 110,000 years. *Nature*, **393**, 54–57.

SIROCKO, F. & LANGE, H. 1991. Clay-mineral accumulation rates in the Arabian Sea during the late Quaternary. *Marine Geology*, **97**, 105–119.

SIROCKO, F., SARNTHEIN, M., ERIENKEUSER, H., LANGE, H., ARNOLD, M. & DUPLESSY, J.C. 1993. Century-scale events in monsoonal climate over the past 24,000 years. *Nature*, **364**, 322–324.

STEENS, T.N.F., KROON, D., TEN KATE, W.G. & SPRENGER, A. 1991. Late Pleistocene periodicities of oxygen isotope ratios, calcium carbonate con-

tents and magnetic susceptibilities of western Arabian Sea margin, Hole 728A. *In:* PRELL, W.L. & NIITSUMA, N. (eds) *Proceedings of the Ocean Drilling Program, Scientific Results, 117*. Ocean Drilling Program, College Station, TX, 309–320.

STOFFERS, P. & ROSS, D.A. 1979. Late Pleistocene and Holocene sedimentation in the Persian Gulf–Gulf of Oman. *Sedimentary Geology*, **23**, 181–208.

STOW, D.A.V., 1977. *Late Quaternary stratigraphy and sedimentation on the Nova Scotian outer continental margin*. PhD thesis, Dalhousie University, Canada.

STOW, D.A.V. & BOWEN, A.J. 1980. Physical model for the transport and sorting of fine-grained sediment in turbidity currents. *Sedimentology*, **27**, 31–46.

STOW, D.A.V. & SHANMUGAM, G. 1980. Sequence of structures in ancient and modern fine-grained turbidites. *Sedimentary Geology*, **25**, 23–42.

STOW, D.A.V. & TABREZ, A. 1998. Hemipelagites: facies, processes and models. Geological Society, London, Special Publications, **129**, 317–338.

STOW, D.A.V. & WETZEL, A. 1990. Hemiturbidite: a new type of deep water sediment. *In: Proceedings of the Ocean Drilling Program, Scientific Results, 116*. Ocean Drilling Program, College Station, TX, 25–34.

STOW, D.A.V., READING, H.G. & COLLINSON, J. 1996. Deep seas. *In:* READING, H.G. (eds) *Sedimentary Environments and Facies, 3rd*. Blackwell Scientific, Oxford, 380–442.

TABREZ, A.R. 1995. *Slope sedimentation around the NW Indian Ocean*. PhD thesis, University of Southampton.

THOUVENY, N. 1988. High resolution paleomagnetic study of late Pleistocene sediments from Baffin Bay: first results. *Canadian Journal of Earth Sciences*, **25**, 833–843.

TUCKER, M.E. 1988. *Techniques in Sedimentology*. Blackwell Scientific, Oxford.

VAN WEERING, T.C.E. & VAN IPEREN, J. 1984. Fine-grained sediments of the Zaire deep-sea fan, southern Atlantic Ocean. *In:* STOW, D.A.V. & PIPER, D.J.W. (eds) *Fine-Grained Sediments: Deep-Water Processes and Facies*. Geological Society, London, Special Publications, **15**, 95–114.

VON RAD, U., SCHAAF, M., MICHELS, K.H., SCHULZ, H., BERGER, W.H. & SIROCKO, F. 1999*a*. A 5000-year record of climatic change in varved sediments from the oxygen minimum zone off Pakistan, NE Arabian Sea. *Quaternary Research*, **51**, 39–53.

VON RAD, U., SCHULZ, H., RIECH, V., DEN DULKE, M., BERNER, U. & SIROCKO, F. 1999*b*. Repeated monsoon-controlled breakdown of oxygen minimum conditions during the past 30,000 years documented in laminated sediments off Pakistan, NE Arabian Sea. *Palaeogeography, Palaeoclimatology, Palaeoecology*, **152**, 129–161.

WALKER, R.G. 1967. Turbidite sedimentary structures and their relationship to proximal and distal depositional environments. *Journal of Sedimentary Petrology*, **37**, 25–43.

WALKER, R.G. 1984. *Facies Models, Geoscience Canada Reprint Series 1, 2nd*. Geological Society of Canada, Waterloo, Ont.

WEEDON, G.P. 1985. Hemipelagic shelf sedimentation and climatic cycles: the basal Jurrassic (Blue Lias) of South Britain. *Earth and Planetary Science Letters*, **76**, 321–375.

WEEDON, G.P. 1989. The detection and illustration of regular sedimentary cycles using Walsh power spectra and filtering, with examples from the Lias of Switzerland. *Journal of the Geological Society, London*, **146**, 133–144.

WHITE, R.S. 1982. Deformation of the Makran accretionary sediment prism in the Gulf of Oman (northwest Indian Ocean). *In:* LEGGETT, J.K. (ed.) *Trench–Forearc Geology: Sedimentation and Tectonics on Modern and Ancient Active Plate Margins*. Geological Society, London, Special Publications, **10**, 357–372.

WHITE, R.S. & LOUDEN, K.F. 1982. The Makran continental margin: structure of a thickly sedimented convergent plate boundary. *AAPG Bulletin*, **34**, 499–518.

WHITE, R.S. & ROSS, D.A. 1979. Tectonics of the western Gulf of Oman. *Journal of Geophysical Research*, **84**, 3479–3489.

WIEDICKE, M., NEBEN, S. & SPIESS, V. 2001. Mud volcanoes at the front of the Makran accretionary complex, Pakistan. *Marine Geology*, **172**, 57–73.